APPROACHING 22% EFFICIENCY WITH MULTICRYSTALLINE N-TYPE SILICON SOLAR CELLS

J. Benick[1], R. Müller[1,2], F. Schindler[1], A. Richter[1], H. Hauser[1], F. Feldmann[1,2], P. Krenckel[1], S. Riepe[1], M. C. Schubert[1], M. Hermle[1], S. W. Glunz[1,2]
[1]Fraunhofer Institute for Solar Energy Systems (ISE), Heidenhofstrasse 2, 79110 Freiburg, Germany
[2]Department of Sustainable Systems Engineering (INATECH), Albert Ludwigs University Freiburg, Georges-Köhler-Allee 103, 79110 Freiburg, Germany

ABSTRACT: The transition to seed assisted growth (high-performance multicrystalline silicon) significantly enhanced the quality of multicrystalline silicon. Combining the new growth technique with the inherent benefits of n-type doping results in a multicrystalline material which should be well suited for the fabrication of high-efficiency solar cells. In this work high-efficiency solar cells with passivating rear contact were fabricated on n-type high-performance multicrystalline silicon, crystallized at Fraunhofer ISE. The material features a high diffusion length >800 µm after application of all high temperature process steps needed for cell fabrication. Applying a black-silicon texture at the font resulted in a weighted reflectance of ~1%, maintaining a good emitter passivation with $J_0 \leq 60$ fA/cm^2 for a 90 Ω/sq emitter. For the resulting n-type multicrystalline silicon solar cells conversion efficiencies up to 22.3% were reached, representing the current record for multicrystalline silicon solar cells.
Keywords: multicrystalline silicon, n-type silicon, high-efficiency solar cells, black silicon

1 INTRODUCTION

Increasing the solar cell conversion efficiency is a powerful lever for a further cost reduction in photovoltaics. To date for industrial screen-printed p-type solar cells on monocrystalline silicon, efficiencies up to 22.6% [1] have been reported, whereas for a comparably processed p-type solar cell on multicrystalline (mc) silicon, the highest certified efficiencies reported to date is 21.3% [2]. Nevertheless, multicrystalline p-type silicon accounts for ~70% of the global solar cell production [3]. Though mc silicon suffers from a higher carrier recombination caused by structural defects and a higher concentration of impurities, the simpler crystallization process of the mc silicon shows a cost advantage potential over monocrystalline silicon. In contrast to marked share, the highest efficiencies for silicon solar cells so far were reported for n-type silicon where for an interdigitated back contact solar cell, a record efficiency of 26.7% was reported [4]. The high material quality of n-type silicon is mainly due to its relative tolerance to common impurities (e.g. Fe) resulting in higher minority carrier diffusion lengths compared to p-type substrates with a similar impurity concentration [5]. With progress in crystallization techniques, such as seed-assisted growth for the fabrication of high-performance multicrystalline silicon (HP mc) [6], the material quality of mc-Si wafers has significantly increased in recent years, mainly due to a reduced density of recombination-active dislocation clusters.

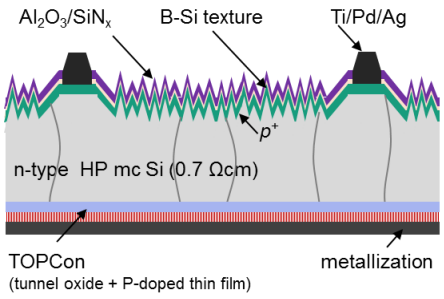

Figure 1: Schematic of the n-type HP mc TOPCon solar cell.

The HP mc process combined with the mentioned benefits of n-type silicon thus might offer opportunities for a low-cost, high-efficiency silicon material which has the potential to reduce the efficiency gap to monocrystalline silicon. In this paper, we apply a high-efficiency solar cell fabrication process with a passivating rear side contact (TOPCon [7]) on high-quality n-type HP mc silicon.

2 n-TYPE SILICON MATERIAL

2.1 Material fabrication

The n-type HP mc silicon applied in this work has been developed at Fraunhofer ISE. The size of the research ingot was G2 which is equivalent to 75 kg of pure polysilicon feedstock. The silicon was crystallized by the directional solidification method with seeded growth. High-purity silicon granules from a Fluidized Bed Reactor (FBR) process were used as seed material and were placed in the bottom of a high-purity fused-silica crucible. As dopant material silicon wafers enriched with phosphorus (1085 ppmw) were used. The crystallization resulted in a resistivity profile from 1.5 Ω cm above the remaining seed material to 0.5 Ω cm at the ingot top. A brick with 156 mm side length was cut from the ingot center. After cropping of 15 mm at bottom and top, the brick was processed into wafers with a thickness of 195 µm by multiwire sawing with SiC slurry and structured wire.

2.2 Material quality

Lifetime samples were fabricated on wafers from the upper ingot part (bulk resistivity of about 0.7 Ω cm) to investigate the electrical quality of the n-type HP mc silicon. The lifetime samples received the same high-temperature processes which are used in the solar cell process sequence, i.e. boron diffusion and annealing of the TOPCon layer. After cleaning (HNO_3, followed by a HF-dip) the lifetime samples received a boron diffusion at 890°C (tube furnace) with one side of the wafer being masked by a PECVD SiO_x. After the diffusion the borosilicate glass and the SiO_x mask were removed in HF and the high temperature step necessary for the annealing of the TOPCon layer was applied (N_2, 800°C). As a last step the boron emitter was removed in a wet-chemical

process and the wafers were passivated by SiN_x.

To characterize the quality of the base material (minority carrier lifetime), photoluminescence imaging calibrated by harmonically modulated photoluminescence [8] was performed. Exemplarily, the lifetime image of the middle part of one n-type HP mc silicon wafer (50×50 mm^2, sister wafer of the 21.9% cell) is shown in Figure 2. The dashed square marks the area where the best solar cell was located on a sister wafer. The measurement was performed at constant illumination of 0.05 suns which is representative for the maximum power point of the fabricated solar cells. The best grains show effective lifetimes >1.5 ms. However, near the grain boundaries, at the boundaries itself and at some defective areas the lifetime is significantly lower. Nevertheless, the average lifetime of the 50×50 mm^2 wafer section shown in Figure 2 (square root harmonic average) is still close to 600 µs. This corresponds to a minority carrier diffusion length of more than 800 µm which is more than 4 times the cell thickness (195 µm). Applying the efficiency limiting bulk recombination analysis (ELBA [9]) on this lifetime sample reveals an efficiency potential of 22.7% in the marked area for the cell structure shown in Fig1. Thus, the applied material (n-type HP mc) should be well suited for the processing of high-efficiency solar cells.

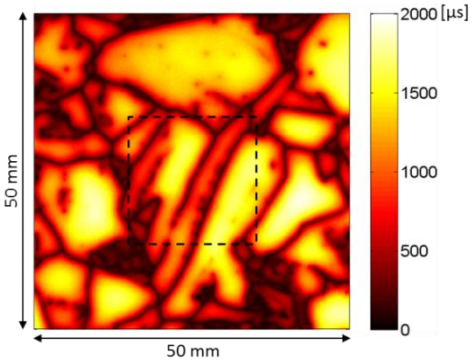

Figure 2: Image of the minority carrier lifetime of an n-type HP mc silicon lifetime sample which received the same high-temperature processes as the final solar cells. The measurement was done at an illumination of 0.05 suns. The marked square in the middle of the shown wafer section indicates the area where the 21.9% cell has been processed on a sister wafer.

3 SURFACE TEXTURE

3.1 Technology

In this work a black silicon texture was realized on the front side of the HP mc silicon solar cells as this surface allows for an almost ideal coupling of the incident light. Fortunately, the previous issue with this texture, the passivation of the nanostructured surface, was solved by an ALD deposition of Al_2O_3 [10–13]. For the realization of the black silicon surface texture an inductively coupled plasma (ICP) process with a very low bias voltage was applied in order to keep the damage as low as possible [14]. This process was performed with an Oxford ICP133 tool using SF_6 and O_2. Note that a separate damage etch back before passivation of the surface is not necessary. A SEM micrograph of the resulting black-silicon texture applied for the solar cells fabricated in this study is shown in Figure 3. As can be seen the ICP texture does not feature perfectly steep needles as known for a "classical" black-silicon texture. The aspect ratio of this texture is in the range of 2.

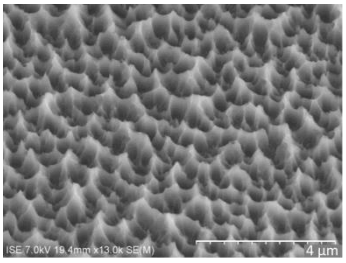

Figure 3: SEM micrograph of the black-silicon front side texture of a HP mc silicon wafer.

3.2 Surface reflection

The reflectance measurement of a wafer with black-silicon texture on the front side and planar back side is shown in Figure 4. Without any antireflection coating the surface reflection weighted with the AM1.5G solar spectrum in the range from 280 to 1000 nm (R_w) is about 2.5%. To further reduce the surface reflection an antireflection coating (ALD Al_2O_3/PECVD SiN_x) was deposited. The ALD process leads to a uniform coating of 10 nm Al_2O_3, whereas the thickness of the SiN_x layer varies between 10 and ~100 nm due to the non-conformality of the PECVD process on the textured surface. Applying the antireflection coating reduces the weighted reflectance to ~1%. Thus, a very effective coupling of the incident light can be reached with the applied surface texture.

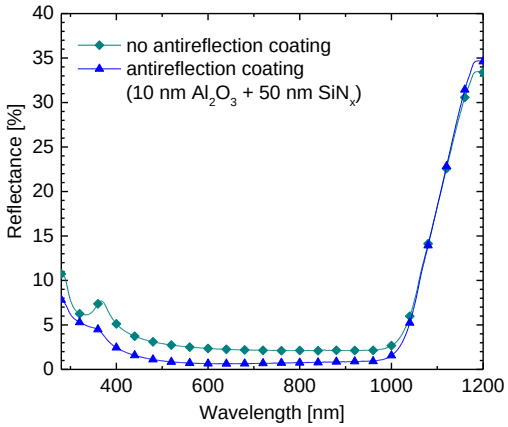

Figure 4: Measured reflectance of the ICP texture (black silicon) without and with antireflection coating.

3.3 Emitter diffusion

As the black-silicon texture has proven to feature very good optical properties, the compatibility of this texture with emitter diffusion and surface passivation has to be verified, too. For this reason lifetime test samples (*n*-type, FZ, 1 or 10 Ω cm) were fabricated. The samples are either planar, feature a both-sides random-pyramids texture or a single side black-silicon texture. All samples received a BBr_3 tube furnace boron diffusion at 890°C (R_{sheet}: 90 Ω/sq, N_{surf}: 8×10^{19} cm^{-3}, depth: 0.3 µm) and were then passivated by PA-ALD deposited Al_2O_3 (10 nm). The saturation current density to quantify the surface recombination was extracted from injection-dependent effective lifetime data measured using QSSPC

[15] according to the high-injection method proposed by [16] and applying the correction routines introduced by [17].

The extracted saturation current densities (for a single surface) are summarized in Table 1. For the planar reference samples a saturation current density in the range of 25 ± 5 fA/cm^2 was measured. For both, random pyramids and black silicon texture the saturation current density is increased to 50 ± 10 fA/cm^2 which still allows for high open-circuit voltages > 700 mV (assuming no additional recombination). Applying no surface passivation (e.g. underneath the metal contacts) the saturation current density of the applied boron emitter (calculated by EDNA [18], 25°C) is approximately ~1100 fA/cm^2.

Table 1: Measured saturation current densities of single surfaces (planar or textured with random pyramids or black silicon). The samples feature the 90 Ω/sq emitter as is also applied for the fabrication of the solar cells.

Surface	J_{0e} [fA/cm^2]
Planar	25 ± 5
Random pyramids	50 ± 10
Black silicon	50 ± 10

4 SOLAR CELLS

4.1 Fabrication

High-efficiency solar cells with passivating rear side contacts (TOPCon [7]) were processed on *n*-type HP mc silicon (195 µm, 0.7 Ω cm, fabricated at Fraunhofer ISE) to investigate the excellent quality of the *n*-type HP mc silicon at the device level. The final cell structure is shown in Figure 1. As references solar cells on float-zone silicon were fabricated as well (*n*-type, 1 Ω cm, 200 µm).

The processing of these *n*-type HP mc TOPCon solar cells starts with the definition and texturing of the active cell area (7 solar cells on each wafer, cell size 20×20 mm^2). The front-side black-silicon texture applied for the HP mc solar cells is realized by a plasma etching step (inductively coupled plasma ICP as introduced earlier). The FZ reference solar cells were textured in a KOH based solution resulting in a random-pyramids surface. To define the cells on every wafer, emitter windows were opened in an oxide mask (PECVD SiO_x) and the uniform boron emitter was realized by the BBr_3 tube furnace diffusion at 890°C (R_{sheet} = 90 Ω/sq). After the removal of the borosilicate glass in HF the passivating rear side contact (TOPCon) was deposited and activated by an annealing step at 800°C. Then the front side was passivated by an Al_2O_3/SiN_x layer stack deposited via PA-ALD and PECVD, respectively. The front side contacts (area fraction ~1.7%) were realized by photolithography and evaporation of a Ti/Pd/Ag layer stack. To improve the electrical contact and completely activate the passivation of front and rear side, the samples received an annealing step in atomic hydrogen (remote plasma hydrogen passivation, 425°C). For the rear side contact, a 1 µm thick Ag layer was evaporated.

4.2 Cell results

The measured IV data of the best cells are summarized in Table 2. As can be seen, for the FZ reference cells high conversion efficiencies up to 23.3% could be reached with a V_{oc} of 684 mV, a J_{sc} of 41.5 mA/cm^2 and a *FF* of 82.2%. The comparison of the measured IV data with 3D total area Quokka [19] device simulations (688.2 mV, 41.6 mA/cm^2, 82.5%) using experimentally-determined input parameters (e.g. $J_{0e,total}$ = 70 fA/cm^2, $J_{0,TOPCon}$ = 7 fA/cm^2, measured reflection, including cell perimeter) reveal that potential of the applied cell structure was almost fully exploited and no significant process-related issues occurred during cell fabrication.

For the *n*-type HP mc silicon solar cells of the first batch also very high conversion efficiencies up to 21.9% were measured with a V_{oc} of 673 mV, a J_{sc} of 40.8 mA/cm^2 and a *FF* of 79.7%. However, there is still a significant gap to the monocrystalline reference solar cells as well as to the efficiency of 22.7% predicted by the analysis of the bulk lifetime (ELBA) of a lifetime sample from a sister wafer to the best solar cell. Thus in the next section a short analysis of the main losses of the first solar cell run will be given. The full loss analysis is still in preparation and will be presented elsewhere.

In a second cell batch the fabrication of the n-type HP mc solar cells with black silicon texture was repeated and a new efficiency record of 22.3% could be achieved. The gain in efficiency is mainly due to small improvements in cell processing like a further reduced surface reflection as well as a lower series resistance.

Table 2: IV measurements (AM1.5g, 100 mW/cm^2, 25°C) of the best cells of each group.

V_{oc} [mV]	J_{sc} [mA/cm^2]	*FF* [%]	*pFF* [%]	η [%]
n-type FZ, random pyramids				
683.9	41.5	82.2	84.1	23.3
n-type HP mc, planar surface				
676.1	37.3	79.5	81.7	20.1
n-type HP mc, black silicon texture				
672.6	40.8	79.7	81.6	21.9*
n-type HP mc, black silicon texture, 2nd run				
674.2	41.1	80.5	81.6	22.3*

* Fraunhofer ISE CalLab (4 cm^2, aperture area)

4.3 Cell analysis (run 1)

The performance of the FZ reference solar cells defines the limit of the cell fabrication process which was used as input for the ELBA analysis. In this case, the cell fabrication process explicitly enables a V_{oc} of 685 mV. According to ELBA, the recombination in the mc-Si bulk material reduces the V_{oc} limit to 679 mV. As ELBA takes the recombination active structural crystal defects into account, these cannot explain the gap between the V_{oc} of the best mc cell (673 mV) and the ELBA limit (679 mV). Thus, the V_{oc}-potential of the material was not fully exploited in this batch - probably due to technological issues - and there is still room for about 6 mV improvement.

The J_{sc} of the mc cells with black-silicon texture is about 0.8 mA/cm^2 lower compared to the FZ reference cells with random pyramids. To investigate this difference, reflection (R) and internal quantum efficiency

(IQE) was measured (see Figure 4). The reflection curve proves that the black silicon texture performs similarly well as the random pyramids. Even the path-length enhancement in the silicon bulk due to the front texture seems to be identical as the reflection from the back side (wavelength range 1000 - 1200 nm) is identical for the black silicon and random pyramids texture. In the low wavelength range, the black silicon shows even superior absorption. So the reason for the lower J_{sc} of the mc cells is not caused by optics but a reduced diffusion length of charge carriers due to the higher recombination rate in the bulk. Holes generated at the back side of the mc cell have a lower chance to reach the emitter at the front side. This is visible by the drop of the internal quantum efficiency above 800 nm (compared to the FZ reference) leading to a reduction in J_{sc}.

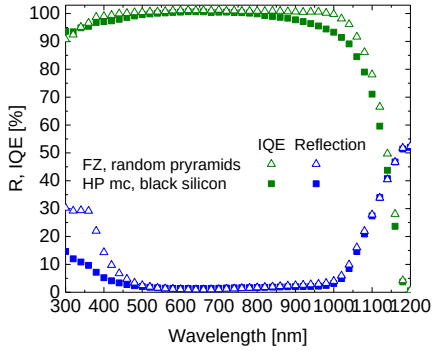

Figure 5: Quantum efficiency and reflection curves of the best *n*-type HP mc solar cell with a black-silicon surface texture as well as of the *n*-type FZ reference with a random-pyramids texture.

The fill factor (*FF*) is often influenced by the series resistance (R_s). In order to separate this effect, SunsV_{oc} measurements were performed to determine the pseudo fill factor (*pFF*) which is not disturbed by R_s. The *pFF* shows that the values of the best cells reach ~84% for the FZ cells and ~82% for the mc cells. No correlation between the *pFF* and the area fraction of RASCD (recombination active structural crystal defects) was found which supports the assumption of a different *pFF* limitation independent of the crystal structure quality.

Whereas the shunt resistance did not lead to a significant loss in *pFF* for the best multicrystalline solar cell, the J_{02} recombination shows a larger influence on the *FF* (~32% of the total recombination at maximum-power point in dark IV measurements). Regarding all multicrystalline cells of the first batch it can be observed that all cells, including the planar ones, exhibit a significantly higher J_{02} than the FZ references. Consequently, the high J_{02} is not an issue of the black-silicon texture, but rather related to the mc-Si material. It can also be observed that the J_{02} does not correlate with the area fraction of recombination active structural crystal defects. Both facts indicate that the high J_{02} might be a more general problem.

Figure 6 shows Suns-V_{oc} curves of the best finished cells together with Suns-$V_{implied}$ curves of the according bulk reference lifetime samples (which received the same high temperature steps as the final solar cells, all diffused areas have been etched) measured with QSSPC. The mc-Si material bulk recombination shows an ideality factor very close to 1 down to 550 mV. However, Suns-V_{oc} measurements of the finished cells reveal that a non-ideal recombination (with ideality factor >1) appears leading to an increased recombination at the maximum-power point (located at 566 mV). From the graphs it becomes obvious, that the mc-Si material is more affected than the FZ material. A possible explanation would be the accumulation of dissolved impurities in (or around) the space charge region during the emitter diffusion. This might lead to the observed non-ideal homogenously distributed recombination that translates into an increased J_{02}.

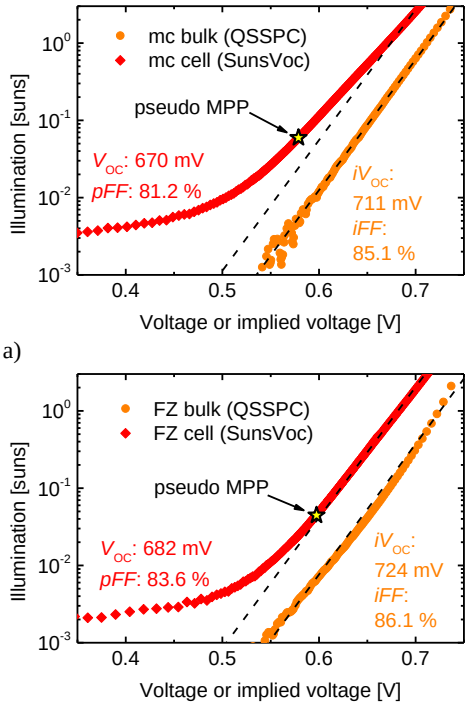

Figure 6: Comparison of the pseudo IV curves of a finished solar cell (Suns-V_{oc}) and a bulk reference lifetime sample, which received the same high temperature processes as the final solar cell (Suns-$V_{implied}$ from QSSPC). Dashed lines indicate the slope of recombination channels with an ideality factor of 1. Measurements are shown for both, the best FZ reference (b) as well as best n-type HP mc silicon solar cell (a).

4 SUMMARY

In this work we could show that n-type HP mc silicon is well suited for the fabrication of high-efficiency solar cells. Applying an adapted TOPCon cell fabrication process with a black-silicon front surface texture and a 90 Ω/sq Al_2O_3-passivated boron emitter a record conversion efficiency of 22.3% could be achieved on the n-type HP mc silicon.

The analysis of the material revealed, that only a part of the efficiency gap to the FZ reference solar cells can be related to recombination active structural crystal defects. A significant portion of the efficiency gap is due to non-ideal recombination, leading to an increased J_{02}. Most probably this might be caused by an accumulation of impurities in the space charge region during emitter diffusion.

ACKNOWLEDGEMENTS

This work was supported by the German Federal Ministry for Economic Affairs and Energy under contract number 0324034 (multiTOP).

The authors would like to thank S. Seitz, A. Seiler, A. Leimenstoll, F. Schätzle, C. Harmel, R. van der Vossen and E. Schäffer for their support with cell processing and measurements.

The authors also would like to thank Wacker Polysilicon for silicon materials and fruitful discussions.

REFERENCES

[1] *Press Releases | Trina Solar*. [Online] Available: http://phx.corporate-ir.net/phoenix.zhtml?c=206405&p=irol-newsArticle&ID=2230468. Accessed on: Feb. 24 2017.

[2] W. Deng *et al.*, "Development of high-efficiency industrial p-type multi-crystalline PERC solar cells with efficiency greater than 21%," *Energy Procedia*, vol. 92, pp. 721–729, 2016.

[3] *Photovoltaics Report - Fraunhofer ISE*. [Online] Available: https://www.ise.fraunhofer.de/de/daten-zu-erneuerbaren-energien.html. Accessed on: Mar. 14 2017.

[4] K. Yoshikawa *et al.*, "Silicon heterojunction solar cell with interdigitated back contacts for a photoconversion efficiency over 26%," *Nat. Energy*, vol. 2, p. 17032, 2017.

[5] D. Macdonald and L. J. Geerligs, "Recombination activity of interstitial iron and other transition metal point defects in p-and n-type crystalline silicon," *Applied Physics Letters*, vol. 85, no. 18, pp. 4061–4063, 2004.

[6] Y. M. Yang *et al.*, "Development of high-performance multicrystalline silicon for photovoltaic industry," *Progress in photovoltaics: research and applications*, vol. 23, no. 3, pp. 340–351, 2015.

[7] F. Feldmann, M. Bivour, C. Reichel, M. Hermle, and S. W. Glunz, "Passivated rear contacts for high-efficiency n-type Si solar cells providing high interface passivation quality and excellent transport characteristics," *Solar energy materials and solar cells*, vol. 120, pp. 270–274, 2014.

[8] J. A. Giesecke, M. C. Schubert, B. Michl, F. Schindler, and W. Warta, "Minority carrier lifetime imaging of silicon wafers calibrated by quasi-steady-state photoluminescence," *Solar energy materials and solar cells*, vol. 95, no. 3, pp. 1011–1018, 2011.

[9] B. Michl *et al.*, "Efficiency limiting bulk recombination in multicrystalline silicon solar cells," *Solar energy materials and solar cells*, vol. 98, pp. 441–447, 2012.

[10] M. Otto *et al.*, "Extremely low surface recombination velocities in black silicon passivated by atomic layer deposition," *Appl. Phys. Lett.*, vol. 100, no. 19, p. 191603, 2012.

[11] P. Repo *et al.*, "Passivation of black silicon boron emitters with atomic layer deposited aluminum oxide," *Phys. Status Solidi RRL*, vol. 7, no. 11, pp. 950–954, 2013.

[12] P. Repo *et al.*, "Effective passivation of black silicon surfaces by atomic layer deposition," *IEEE Journal of Photovoltaics*, vol. 3, no. 1, pp. 90–94, 2013.

[13] M. Algasinger *et al.*, "Improved black silicon for photovoltaic applications," *Advanced Energy Materials*, vol. 3, no. 8, pp. 1068–1074, 2013.

[14] J. Hirsch, M. Gaudig, N. Bernhard, and D. Lausch, "Optoelectronic properties of Black-Silicon generated through inductively coupled plasma (ICP) processing for crystalline silicon solar cells," *Applied Surface Science*, vol. 374, pp. 252–256, 2016.

[15] R. A. Sinton and A. Cuevas, "Contactless determination of current–voltage characteristics and minority-carrier lifetimes in semiconductors from quasi-steady-state photoconductance data," *Applied Physics Letters*, vol. 69, no. 17, pp. 2510–2512, 1996.

[16] D. E. Kane and R. M. Swanson, "Measurement of the emitter saturation current by a contactless photoconductivity decay method," in *18th IEEE photovoltaic specialists conference 1985*.

[17] A. Kimmerle, J. Greulich, and A. Wolf, "Carrier-diffusion corrected J0-analysis of charge carrier lifetime measurements for increased consistency," *Solar energy materials and solar cells*, vol. 142, pp. 116–122, 2015.

[18] K. R. McIntosh and Pietro P. Altermatt, "A freeware 1D emitter model for silicon solar cells," in *35th IEEE Photovoltaic Specialists Conference (PVSC), 2010*.

[19] A. Fell, "A Free and Fast Three-Dimensional/Two-Dimensional Solar Cell Simulator Featuring Conductive Boundary and Quasi-Neutrality Approximations," *IEEE Trans. Electron Devices*, vol. 60, no. 2, pp. 733–738, 2013.